Determination of the Solution Structure of a Platelet-Adhesion Peptide of von Willebrand Factor

Heather M. Knott,[‡] Michael C. Berndt,[§] Andrew V. Kralicek,[‡] Séan I. O'Donoghue,[‡] and Glenn F. King*,[‡]

Department of Biochemistry, University of Sydney, Sydney, New South Wales 2006, Australia, and Vascular Biology Laboratory, Baker Medical Research Institute, Melbourne, Victoria 3181, Australia

Received April 21, 1992; Revised Manuscript Received July 24, 1992

ABSTRACT: Two-dimensional nuclear magnetic resonance (NMR) spectroscopy in combination with distance geometry (DG) and dynamical simulated annealing (DSA) calculations have been used to determine the tertiary solution structure of a synthetic 29-residue fragment of von Willebrand factor (vWF). This fragment (D514–E542) represents an adhesion site on vWF for its platelet receptor, the glycoprotein Ib–IX complex (GP Ib–IX). The NMR data yielded 109 interproton distance measurements and two χ_1 dihedral angle constraints for use in DG and DSA calculations. Most prominent in the calculated family of solution structures was an amphipathic, right-handed α-helix in the C-terminal segment of the peptide. We propose that this highly structured region may be important for the specific molecular interaction of vWF with the GP Ib–IX complex.

von Willebrand factor (vWF)[1] is an adhesive plasma glycoprotein which mediates platelet adhesion to exposed vascular subendothelial matrix (Sakariassen et al., 1979). It is generally believed that, under conditions of high shear stress, the binding of vWF to damaged blood vessel walls exposes an otherwise 'cryptic' binding site on vWF for a specific platelet-surface receptor, the GP Ib-IX complex (Ali-Briggs et al., 1981; Berndt et al., 1988; Berndt, 1989); however, the molecular mechanism of this interaction is unknown. This adhesive event not only constitutes the initial stage in haemostasis but is also clearly instrumental in the pathogenesis of vascular disease such as atherosclerosis and coronary thrombosis. Platelet adhesion, and hence the structure and function of vWF, therefore represents an important area for the potential development of anti-thrombotic therapies.

The mature vWF protein has a subunit molecular weight of 275 kDa consisting of 2050 amino acid residues (Titani et al., 1986) and circulates in plasma as a series of disulfide-linked multimers ranging in molecular weight from $\sim 1 \times 10^6$ to 20×10^6 kDa (Girma et al., 1987). Analysis of proteolytic fragments of vWF has localized the binding domain for its platelet adhesion receptor, the GP Ib–IX complex, to the first A-domain repeat of vWF and adjacent sequences between V449 and K728 (Fujimara et al., 1986; Andrews et al., 1989). Recent studies have further identified candidate peptide sequences within this fragment that mediate the interaction of vWF with the GP Ib-IX complex or with in vitro modulators such as botrocetin and ristocetin (Mohri et al., 1988; Sugimoto et al., 1991; Berndt et al., 1992). In particular, we have identified a 29-residue sequence within the first A-domain of vWF (vwf29; D514-E542) which appears to be important in vWF recognition by the human platelet GP Ib-IX complex (Berndt et al., 1992). This paper presents a tertiary solution structure of vwf29, obtained using 2D ^{1}H NMR spectroscopy in combination with DG and DSA calculations. We propose that an amphipathic α-helix observed in the C-terminal portion of vwf29 represents an important structural motif in the interaction of vWF with the platelet GP Ib-IX receptor.

MATERIALS AND METHODS

Materials. The two peptides, vwf29 (DLVFLLDGSS-RLSEAEFEVLKAFVVDMME) and vwf16c (E527–E542; EAEFEVLKAFVVDMME), were synthesized by Auspep Pty. Ltd. (Melbourne, Australia). Both peptides were carboxylated at the amino-terminus and amidated at the carboxy-terminus. 3-Trimethylsilyl[2,2,3,3-^{2}H]propionate (TSP-d_4) was obtained from Fluka A.G. (Buchs, Switzerland). The DG program DIANA was kindly provided by Dr Peter Güntert (Güntert et al., 1991) while the molecular dynamics program X-PLOR was obtained from Professor Axel Brünger (Brünger, 1990). Molecular superpositions were performed using the SUPPOS program from the Gröningen BIOMOL protein structure package. The program uses the method of Kabsch (1976) to calculate the rotation for optimal superposition of a pair of structures. All structure calculations and molecular superpositions were performed on a Sun SPARCstation 2GX. Molecular graphics were displayed on a Silicon Graphics IRIS 4D/20 workstation using the MidasPlus software package obtained from the Computer Graphics Laboratory, University of California, San Francisco (Ferrin et al., 1988).

Sample Preparation. Initially the peptide samples were lyophilized to remove any excess acetate from the chemical syntheses. Peptides were then dissolved in 90%H_2O/10%D_2O to a total volume of 600μL at concentrations of $\sim$2.1 mM for vwf29 and $\sim$3.0 mM for vwf16c. Azide (0.8 mM) was added to both samples to inhibit bacterial growth. Final solutions were filtered (0.45-μm filters) into high-precision, 5-mm outer-diameter NMR tubes and the pH was adjusted using dilute HCl and NaOH.

NMR Experiments. One-dimensional spectra (consisting of 128 scans of 16 384 data points each) were acquired at both 303 and 310 K, over a pH range of 7.20–6.03 for vwf29

* Address correspondence to this author.
‡ University of Sydney.
§ Baker Medical Research Institute.

[1] Abbreviations: DG, distance geometry; DQF-COSY, double-quantum-filtered correlated spectroscopy; DSA, dynamical simulated annealing; FID, free induction decay; GP Ib–IX complex, glycoprotein Ib–IX complex; HOHAHA, homonuclear Hartmann–Hahn spectroscopy; NMR, nuclear magnetic resonance; nOe, nuclear Overhauser effect; NOESY, nuclear Overhauser effect spectroscopy; rf, radiofrequency; RMSD, root mean squared deviation; ROESY, rotating-frame Overhauser effect spectroscopy; τ_m, mixing time; TSP-d_4, 3-trimethylsilyl[2,2,3,3-^{2}H]propionate; vWF, von Willebrand factor.

0006-2960/92/0431-11152$03.00/0

and 7.26–6.05 for vwf16c. The most acidic pH values used were the lowest at which the peptides were completely soluble. All 1D spectra were apodized using a Lorentz–Gauss function prior to Fourier transformation.

Phase-sensitive 2D spectra were acquired on either a Bruker AMX-400 wide-bore or AMX-600 narrow-bore spectrometer using time-proportional phase incrementation (Marion & Wüthrich, 1983). The spectra were collected at 303 K and the sample was not spun in any experiment. The spectral widths were 5.6–5.7 and 3.6–4.0 kHz at 600 and 400 MHz, respectively. Acquisition incorporated a 1.4–1.6-s relaxation delay during which time the water resonance was coherently irradiated with a continuous, low-power pulse. The water resonance was similarly irradiated during all NOESY mixing times.

A total of 420–512 FIDs, each consisting of 64–128 summed transients in 4096 data points, were collected for each 2D spectrum. All raw data were zero-filled to a final data matrix of 4096 ($F2$) × 1024 ($F1$) real data points. Prior to Fourier transformation, the data were apodized by using a Lorentz–Gauss function in $F2$ (LB = −20, GB = 0.2) and a pure cosine bell function in $F1$ or by using a shifted sine bell function in both dimensions. Baseline correction, using a third-order polynomial, was applied in both dimensions and chemical shift values were referenced to the methyl protons of TSP-d_4 at 0.00 ppm.

Two-dimensional HOHAHA spectra were collected using a 100-ms MLEV-17 spin-lock mixing sequence (Bax & Davis, 1985) with trim pulses of 2.5 ms. The field strength of the spin-lock was ~9–10 kHz. Two-dimensional ROESY spectra were acquired with a 2–4-kHz rf field strength.

For vwf29 and vwf16c, a number of 2D dipolar coupling experiments (NOESY and ROESY, respectively) were collected in order to facilitate sequence-specific assignments. Experiments were collected over a range of mixing times (τ_m = 150–400 ms for vwf29 and τ_m = 100–250 ms for vwf16c) to establish the effect of spin-diffusion on the experimental data. For vwf29, the 350-ms NOESY was chosen for compilation of distance constraints since it represented a suitable compromise between reasonable cross-peak intensity and minimal spin-diffusion effects. Cross-peak intensities, determined by counting contour levels and/or volume integration, were converted to interproton distance ranges as discussed below.

The $^3J_{NH\alpha CH}$ coupling constants for vwf29, measured from antiphase peak splitting in DQF-COSY spectra, were all within the range 5–9 Hz and therefore provided no unique ϕ angle constraints for DG calculations. However, the methyl groups of V3 and V19 were stereospecifically assigned from measurement of $^3J_{\alpha\beta}$ coupling constants and αCH–γCH nOe intensities (Basus, 1989).

Structure Determination. For vwf29, 184 intra- and interresidue distance constraints were obtained from the 350-ms NOESY spectrum. These constraints were input to the DG program DIANA as upper limits on the distance between the dipolar-coupled protons: 2.8 Å (strong nOes), 3.3 Å (medium nOes), and 4.5 Å (weak nOes), with the lower distance constraints set by the van der Waals radii. DIANA filtered these to 93 relevant structural constraints; i.e., ^1H–^1H distances which were independent of conformation or for which there was no conformation which violates the set distance limit were excluded from the calculations (Güntert et al., 1991). Furthermore, stereospecific assignment of the γCH's of V3 and V19 provided χ_1 dihedral angle constraints for these two residues. These angles were constrained between

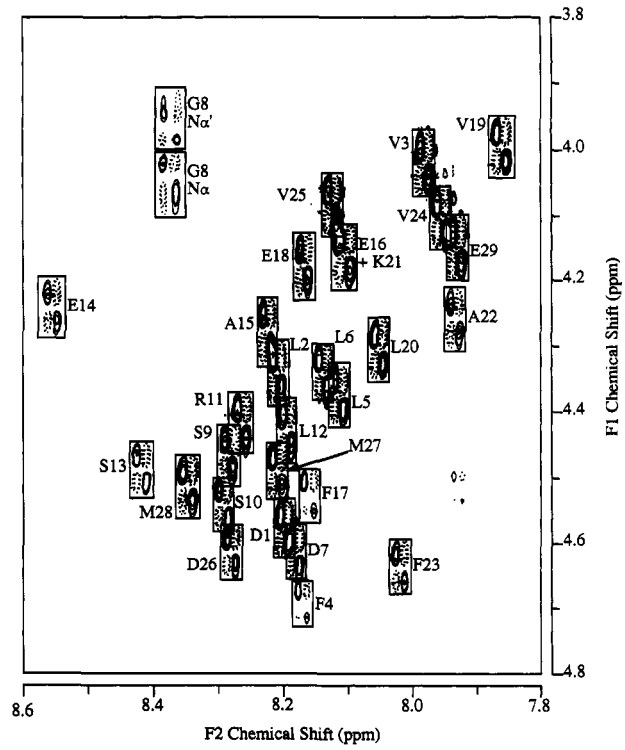

FIGURE 1: Fingerprint region of a phase-sensitive DQF-COSY spectrum of vwf29. Scalar connectivities between the NH and αCH for all 29 residues can be seen, although those of E16 and K21 are degenerate. Positive and negative contours are shown as solid and dotted lines, respectively.

150° and 210°.

DIANA was used in conjunction with GLOMSA, a program which enables stereospecific assignments to be made by comparison of the distance constraints, including arbitrary stereospecific assignments, with preliminary DIANA structures. GLOMSA then calculates (on the basis of constraint violations) whether the assignment is correct, should be reversed, or cannot be defined (Güntert et al., 1991). The 10 best structures from an individual DIANA run, using the 93 distance constraints, were input to GLOMSA. Additional stereospecific assignments made by this method were then added to the DIANA upper limits file and more DIANA structures were generated. Using these two programs (DIANA and GLOMSA) iteratively, an extra 16 upper-limit distance constraints were obtained (109 in total) due to stereospecific assignment of the β-methylene protons of E16, F17, L20, F23, and D26 and the δ-methyl groups of L20. A final set of 600 DIANA structures was generated, using the final list of 109 distance constraints and two χ_1 angles, and the best 50 structures (on the basis of the value of the variable target function) were used for further refinement.

The structures were refined in X-PLOR using the dynamical simulated annealing method described by Clore and co-workers (Nilges et al., 1988; Clore & Gronenborn, 1989). Stage 1 of the protocol consists of 50 cycles of energy minimization using the standard X-PLOR parameters for restraining the covalent geometry [k_{bond} = 500 kcal·mol^{-1}·Å^{-2}, k_{angle} = 500 kcal·mol^{-1}·rad^{-2}, $k_{improper}$ = 500 kcal·mol^{-1}·rad^{-2}, k_{dihed} = 0 kcal·mol^{-1}·rad^{-2}; see Brünger (1990)] plus the experimental constraints on interatomic distances and χ_1 angles (k_{nOe} = 60 kcal·mol^{-1}·Å^{-2} and k_{cdihed} = 50 kcal·mol^{-1}·rad^{-2}). For this stage, nonbonded interactions were modeled by a weak "repel" function which ignores electrical interactions and allows atoms to pass through each other (repel = 1.0 and C_{rep} = 0.002

Table I: Chemical Shift Values for vwf29 and vwf16c[a]

residue	NH	αCH	α'CH	βCH	β'CH	γCH	γ'CH	δCH	δ'CH	εCH	2,6H	3,5H	4H
D1	8.23	4.55		2.66	2.54								
L2	8.23	4.32		1.60	1.47			0.93	0.87				
V3	7.99	4.00		1.97		0.86	0.82						
F4	8.18	4.69		3.07	2.98						7.24	7.39	7.34
L5	8.12	4.34		1.54				0.89	0.84				
L6	8.15	4.34		1.64	1.54			0.93	0.87				
D7	8.19	4.59		2.77	2.70								
G8	8.39	4.01	3.94										
S9	8.30	4.44		3.95	3.89								
S10	8.28	4.51		3.87									
R11	8.28	4.39		1.86	1.74	1.61		3.18					
L12	8.20	4.40		1.63				0.91	0.85				
S13	8.45	4.47		4.02	3.93								
E14	8.58	4.22		2.10	2.01	2.32							
	8.30	*4.22*		*b*	*b*	*b*							
A15	8.25	4.26		1.38									
	8.37	*4.30*		*1.35*									
E16	8.10	4.14		1.99		2.23	2.16						
	8.30	*4.18*		*1.90*		*b*	*b*						
F17	8.18	4.49		3.19	3.09						7.25 (3)	7.33 (8)	7.30 (3)
	8.04	*4.61*		*3.21*	*3.06*						*b*	*b*	*b*
E18	8.18	4.14		2.01		2.28							
	8.22	*4.24*		*b*		*b*							
V19	7.86	3.97		2.11		1.01	0.95						
	8.02	*4.03*		*2.08*		*0.93*							
L20	8.06	4.27		1.65	1.59			0.92	0.86				
	8.17	*4.34*		*1.65*	*1.61*	*1.64*		*0.92*	*0.86*				
K21	8.13	4.14		1.72	1.65	1.37		1.62		2.94			
	8.12	*4.24*		*1.72*		*1.39*		*1.68*		*2.98*			
A22	7.93	4.23		1.31									
	8.04	*4.27*		*1.30*									
F23	8.03	4.61		3.16	3.06						7.24 (8)	7.34 (3)	7.29 (9)
	8.06	*4.64*		*3.04*							*b*	*b*	*b*
V24	7.97	4.08		2.04		0.93							
	7.96	*4.11*		*2.02*		*0.88*							
V25	8.14	4.07		2.07		0.96							
	8.12	*4.07*		*2.08*		*0.96*							
D26	8.29	4.59		2.70	2.61								
	8.31	*4.59*		*2.69*	*2.61*								
M27	8.21	4.47		2.09	2.02	2.57	2.53						
	8.29	*4.45*		*2.04*		*2.55*							
M28	8.35	4.47		2.14	2.04	2.62	2.58						
	8.39	*4.46*		*2.10*		*2.77*							
E29	7.93	4.12		2.15		2.23							
	8.31	*4.25*		*b*		*b*							

[a] Chemical shift values were generally determined from antiphase peak splitting in DQF-COSY spectra and were referenced to the methyl protons of TSP-d_4 at 0.00 ppm. Chemical shift values for vwf29 and vwf16c are in plain text and italics, respectively. [b] Not assigned due to spectral overlap.

kcal·mol^{-1}·Å^{-4}). In stage 2, the initial atomic velocities are chosen from a Maxwellian distribution at 1000 K and the dynamic trajectory is followed for 15 ps in 2-fs steps. During stage 3, the nonbonded repel term (C_{rep}) is increased exponentially (to 0.1 kcal·mol^{-1}·Å^{-4}) and the nOe restraint term (asymptote) is increased linearly (to 1.0) over 9 ps. In stage 4, the system is cooled from 1000 to 300 K (repel = 0.8 and C_{rep} = 4 kcal·mol^{-1}·Å^{-4}) over 2.8 ps. During stage 5, the system is equilibrated at 300 K for 1 ps using Lennard–Jones and Coulomb potentials for nonbonded interactions (repel = 0). This is followed by 1000 cycles of restrained energy minimization (stage 6).

RESULTS

Spectral Assignment. For both peptides, the similarity of 1D spectra (data not shown) across all pH values demonstrated that there were no substantial changes to the native structures of these peptides over the conditions studied, ranging from pH ~7.2 (physiological) to the low pH required to observe the labile amide protons.

The DQF-COSY fingerprint region of vwf29 is shown in Figure 1; an α*CH*–N*H* scalar connectivity is observed for each of the 29 residues in this peptide, although those of E16 and K21 are coincident. As well as the unique residues in this peptide (i.e., G8, R11, and K21), complete residue-specific spin-system assignment was possible for the two alanyls (A15 and A22) and the four valyls (V3, V19, V24, and V25) according to their unique connectivity patterns. Complete spin-system assignment was also made for the five leucine residues (L2, L5, L6, L12, and L20). The glutamyls (E14, E16, E18, and E29) and methionyls (M27 and M28) were assigned on the basis of the different chemical shifts of the β- and γ-protons of these residues (see Table I). These assignments were confirmed by the relayed connectivities observed in the HOHAHA experiment. The nine AMX spin systems were tentatively assigned in the scalar coupling experiments on the basis of different chemical shifts. However, NOESY experiments were required to confirm these, particularly the complete assignment of the Phe residues, made possible by the dipolar connectivity between the aromatic ring and aliphatic side-chain protons of these residues.

Identification of sequential N*H*–α*CH* connectivities between every neighboring pair of residues except D1–L2, L5–L6, S9–S10, R11–L12, F17–E18, V24–V25, and M27–M28

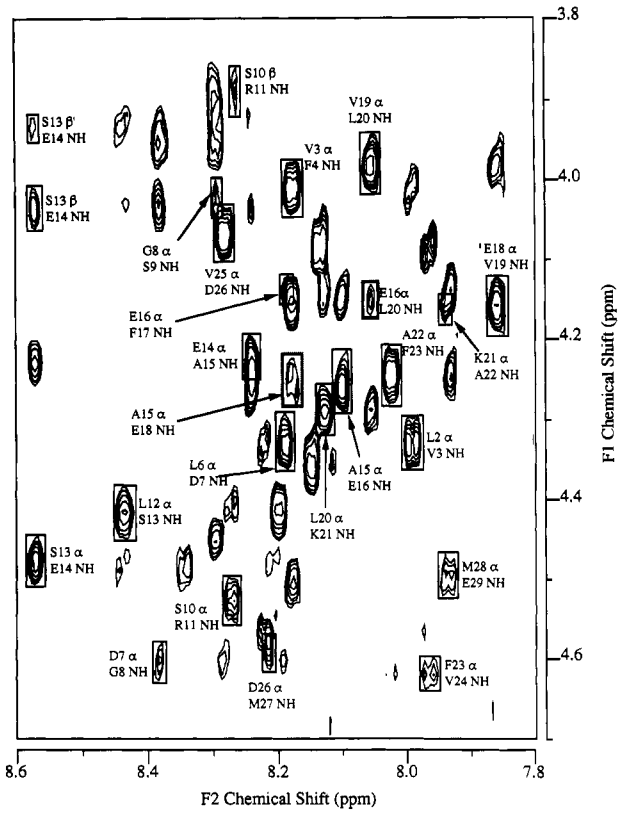

FIGURE 2: Fingerprint region of a 350-ms NOESY spectrum of vwf29. Boxes with thin outlines enclose sequential connectivities between the αCH and NH protons of neighboring residues, while boxes with thick outlines enclose medium-range αCH–NH connectivities. Unlabeled peaks are those involving intraresidue dipolar connectivities or those considered to be due to spin diffusion.

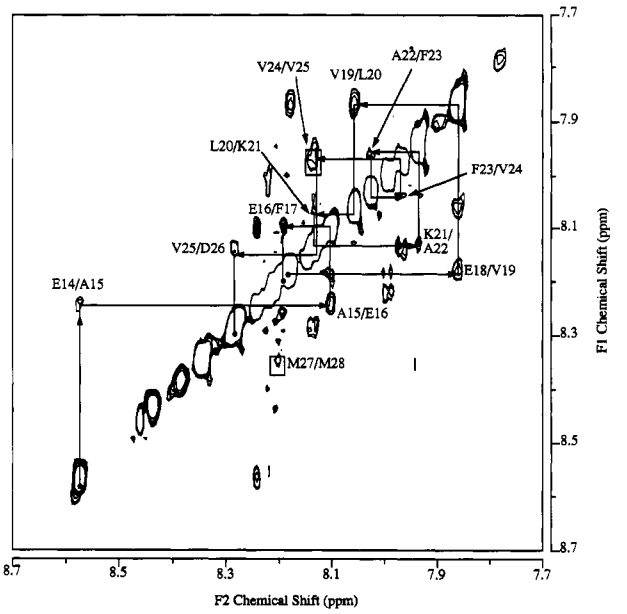

FIGURE 3: Amide proton region of a 350-ms NOESY spectrum of vwf29. The continuous lines connect nondegenerate, sequential NH–NH dipolar couplings from E14 to F17 and from E18 to D26.

(due to degeneracy of the chemical shift values of these protons) enabled complete sequence-specific assignment of vwf29 (see Figure 2). Sequential NH–NH connectivities ($NN_{i,i+1}$) were also observed for all nondegenerate residues between L2 and L6 and between E14 and E29 (except D26–M27), suggesting defined secondary structure for at least the C-terminal region of the peptide (Figure 3). Furthermore, the NOESY experiments demonstrated a number of interresidue connectivities ranging from sequential ($d_{i,i+1}$) to medium-range ($d_{i,i+3}$ and $d_{i,i+4}$); these are summarized in Figure 4a. The $d_{i,i+3}$ connectivities are specific to a region between E14 and V25 and are indicative of α- or 3_{10}-helical structures. Particularly noticeable in the NOESY spectra were intense cross-peaks between the ring protons of both F17 and F23 and the βCH, δCH, and $\delta' CH$ of L20 (all $d_{i,i+3}$ connectivities), suggesting that this helical segment is stabilized by hydrophobic interactions between the side chains of these three residues.

Pastore and Saudek (1990) have shown that regions of α-helical secondary structure are characterized by upfield (arbitrarily designated positive) displacements of the αCH chemical shifts from their random coil positions; these displacements are most easily discerned using a "smoothing function" of ±2, whereby the αCH chemical shift displacement of a residue is averaged with that of its two N- and C-terminal neighbors. The αCH chemical shift displacements for vwf29 obtained using this smoothing function are shown in Figure 4b. The large positive displacements (>0.1) observed in the region A15–M28 are good circumstantial evidence of α-helical secondary structure in this region. This is further supported by the $d_{i,i+4}$ connectivity observed between E16 and L20.

DQF-COSY, HOHAHA, and ROESY experiments performed on vwf16c enabled near-complete sequence-specific assignment of the peptide. Spin systems were assigned by comparison with vwf29 spectra and with random coil chemical shift values and spin-system patterns (Wüthrich, 1986). It was not possible to fully assign the βCH–γCH region (1.8–2.3 ppm) of the four glutamyls (E14, E16, E18, and E29) or the aromatic ring protons of the two Phe residues. Chemical shift values for this peptide are shown in Table I. The graphs in Figure 5 show the deviation of the αCH chemical shifts of the peptides from that for random coil peptides (Wüthrich, 1986). The similarity of the graphs for vwf16c and the C-terminal portion of vwf29 strongly suggests that the smaller fragment adopts a conformation similar to that of the corresponding region of vwf29.

Calculation of Solution Structure of vwf29. Of the 50 structures refined using DSA, 20 were chosen as representative of the solution structure of vwf29 on the basis of the summed violations of the NMR constraints, the final values of the Lennard–Jones pontential (E_{L-J}), and the deviations from ideal bond lengths and angles. The initial structures had poor nonbonded contacts [mean $E_{L-J} = (4 \pm 5) \times 10^6$ kcal·mol^{-1}] and small deviations from idealized covalent geometry (mean rms deviations of the bond lengths and bond angles from idealized geometry of 0.03 ± 0.03 Å and 2.6° ± 1.1°, respectively). The final structures had good nonbonded contacts as evidenced by the negative Lennard–Jones potential (mean $E_{L-J} = -100 \pm 7$ kcal·mol^{-1}) and better covalent geometry (mean rms deviations of the bond lengths and bond angles from idealized geometry of 0.005 ± 0.001 Å and 1.86° ± 0.12°, respectively). The pseudopotential accounting for the NMR restraints was also substantially reduced during the DSA refinement from a mean of 60 ± 19 to 9.5 ± 2.1 kcal·mol^{-1}. On average, the final family of 20 structures had ~5 violations of the NMR-derived distance constraints per structure. Of these violations, >90% were below 0.20 Å.

Figure 6 shows a stereoview of the backbone atoms (N, C, and Cα) of the family of 20 vwf29 structures generated by the combined DG/DSA calculations. The structures are superimposed, against a mean structure calculated by coordinate averaging, for minimum root mean squared deviation (RMSD) over the region A15–V24. RMSDs among the family were obtained by taking the mean ± standard deviation

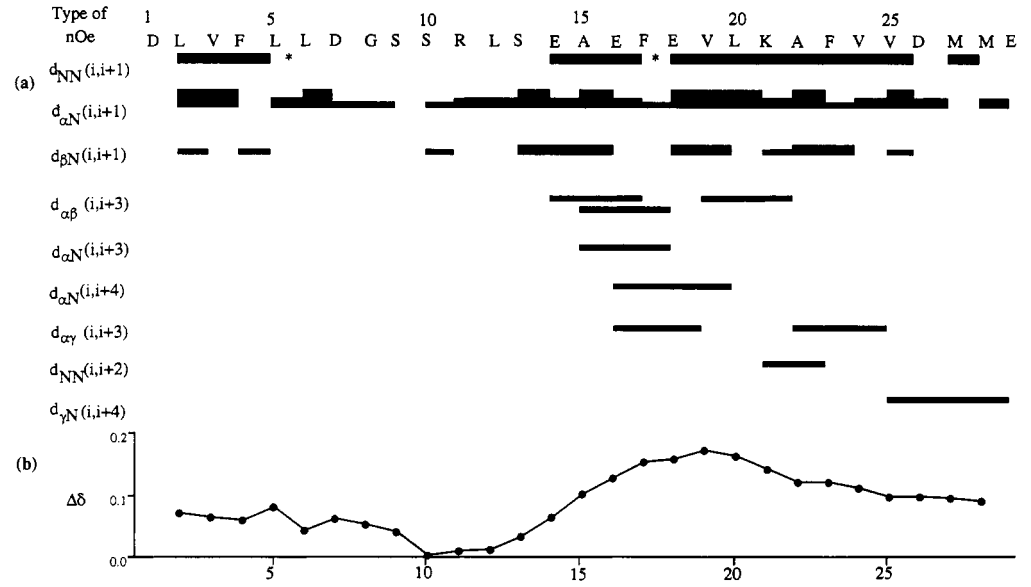

FIGURE 4: (a) Summary of interresidue nOes for vwf29. Interresidue nOes are denoted by a solid box and the height of the box is proportional to nOe intensity. Asterisks indicate nOes that could not be observed due to degeneracy of the chemical shifts of the protons involved. Note that all but one of the nonsequential nOes are observed in the region E14–V25. (b) Deviation of the αCH chemical shifts from random coil values for vwf29. The graph was smoothed according to the method of Pastore and Saudek (1990), using a window function of ±2 residues. The terminal residues (D1 and E29) were excluded from the calculations to eliminate possible end effects due to N-terminal acetylation and C-terminal amidation.

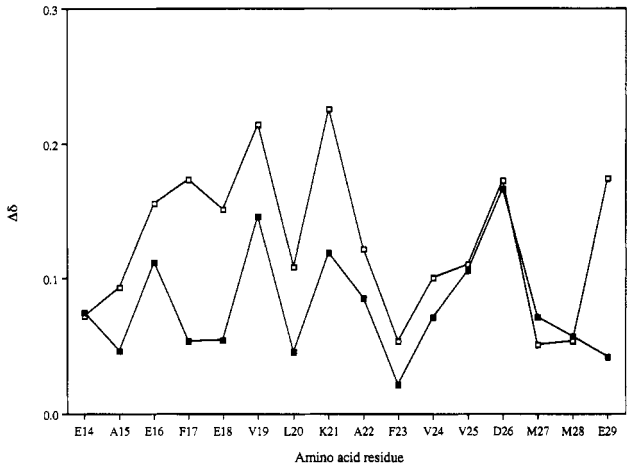

FIGURE 5: Deviation of the αCH chemical shift values of vwf16c (■) and the C-terminal region of vwf29 (□) from those for random coil peptides. The similarity of the graphs indicates that the smaller peptide probably adopts a conformation similar to that of the corresponding region of vwf29.

of the pairwise RMSDs obtained between each of the structures and the mean structure. Clearly the N-terminal 13 residues (D1–S13) and C-terminal four residues (D26–E29) are poorly defined and probably represent highly dynamic segments of the peptide, consistent with the paucity of NMR constraints obtained for these regions. As a consequence, the RMSDs for the entire molecule are very large: 6.3 ± 1.0 Å for all atoms and 5.4 ± 1.1 Å for the main-chain atoms only (N, C, Cα, and O). Conversely, the region E14–V25 is well defined, forming approximately three turns of right-handed α-helix; the RMSDs for this region, 1.22 ± 0.18 Å for all atoms and 0.49 ± 0.18 Å for the main-chain atoms only, are much lower than those for the whole molecule. These results reflect the distribution of NMR-derived conformational constraints; on average, the conformation of each residue is defined by ~3 constraints for the regions D1–S13 and D26–E29 and by ~12 constraints for the region E14–V25.

DISCUSSION

The previous paper (Berndt et al., 1992) showed that a 29-residue segment of vWF spanning from D514 to E542 (vwf29) strongly inhibited the ristocetin- and botrocetin-induced binding of vWF to platelets and thus was likely to encompass and at least partially maintain the conformation of the recognition site on vWF for the platelet GP Ib–IX receptor. In this study, we have determined the solution conformation of vwf29 using NMR spectroscopy. The prominent feature of the calculated tertiary solution structure of vwf29 is approximately three turns of right-handed α-helix extending from E527 to V538. The αCH chemical shift values and interresidue dipolar connectivities observed for vwf16c (E526–E542) indicate that this peptide is probably similarly structured in this region. In contrast, the N-terminal 13 residues and the C-terminal four residues are poorly defined, suggesting conformational flexibility in solution for these regions of the peptide. In intact vWF, however, the segment D514–S526 might be conformationally restrained due to the adjacent C509–C695 intrasubunit disulfide bond (Andrews et al., 1989).

Although vwf29 is a strong inhibitor of vWF–GP Ib–IX complex interaction, the truncated peptides D514–E529, D520–D539, and E527–E542 (vwf16c) are much less active (Berndt et al., 1992), suggesting that both the N- and C-terminal segments of vwf29 are involved in GP Ib–IX recognition. In terms of the homology of this sequence with other A-domain proteins, it is therefore interesting to speculate that the highly conserved segment D514–S522 might represent a general recognition sequence whereas sequence variability in the α-helical region E527–V538 might confer receptor specificity.

Closer examination of the α-helical segment (E14–V25) of the family of 20 superimposed structures of vwf29 shows an interesting disposition of charged and hydrophobic residues around the helix backbone. F17, L20, and F23 appear to form a hydrophobic face on one side of the α-helix while the less apolar residues (A15, V19, and A22) span another face (Figure 7a). Furthermore, several charged residues (E14,

FIGURE 6: Stereoview of the backbone atoms (N, C, and Cα) of the family of 20 structures representing the tertiary solution structure of vwf29. The structures were superimposed for minimum RMSD over the region A15–V24. The N- and C-termini of one structure are labeled.

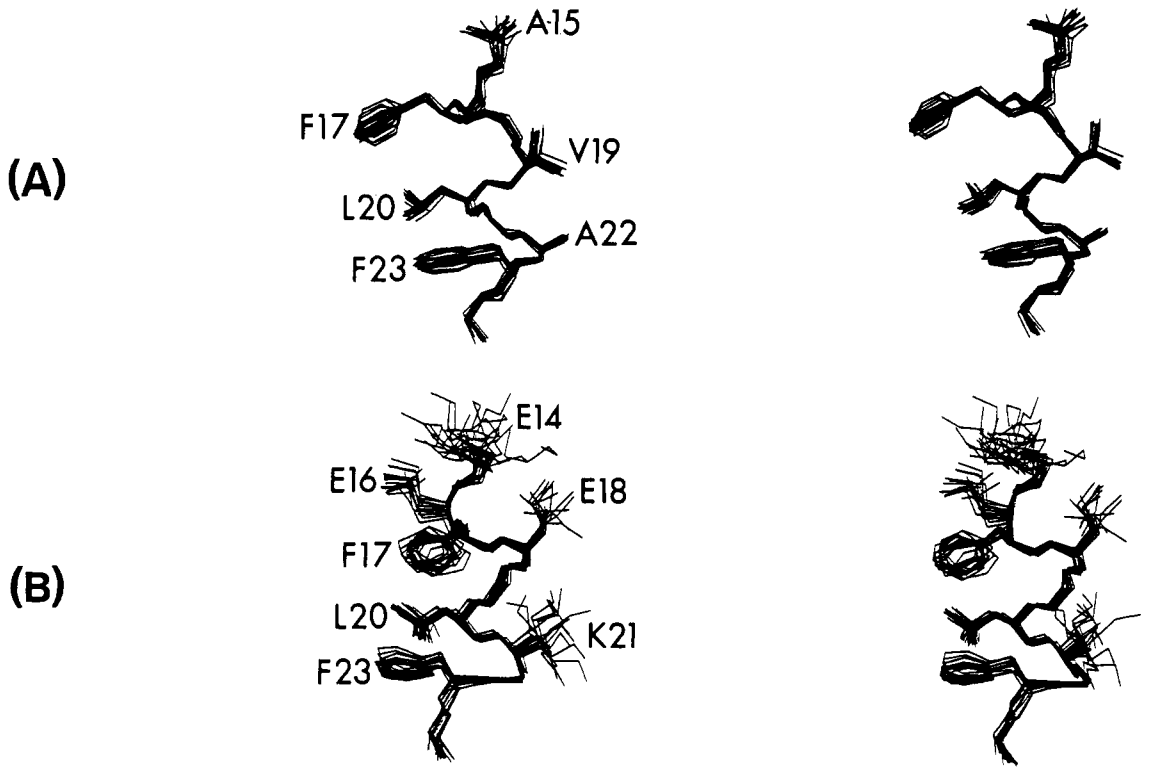

FIGURE 7: Stereoviews of the α-helical segment of vwf29. The family of 20 calculated vwf29 structures were superimposed for minimum RMSD over the region A15–V24. (a) Lateral view of the helix showing the backbone atoms (N, C, and Cα) of residues A15–V24 as well as a heavy-chain representation of the side-chain atoms of the hydrophobic (F17, L20, and F23) and weakly apolar (A15, V19, and A22) residues. (b) Lateral view of the helix (E14–V24) demonstrating the disposition of hydrophobic (F17, L20, and F23) and charged (E14, E16, E18, and K21) residues.

E18, and K21) lie along a third face of the helix (Figure 7b), thus making it highly amphipathic.

Site-directed mutagenesis of the Ib α-chain of the platelet GP Ib–IX receptor has localized a highly acidic region which appears to be responsible for the specific molecular interaction of platelets with vWF. This segment extends from S251 to A302 and contains 10 Glu/Asp residues in the region D269–D287 which, when mutated to Gln/Asn residues, severely impair botrocetin- and ristocetin-mediated vWF binding to platelets (Murata et al., 1991). Thus, it appears likely that electrostatic interactions may be largely responsible for the interaction of vWF with the platelet GP Ib–IX receptor. However, it is unlikely that this region of GP Ibα interacts directly with the helical segment of vwf29 since the only charged face of this amphipathic helix is also largely acidic, comprising residues E527, E531, and K534.

Recent evidence suggests that the 36 residues immediately downstream of vwf29 (i.e., R543–R578) are critically involved in the regulation of vWF adhesive function. vWF from patients with the rare IIb subtype of von Willebrand's disease can bind spontaneously to the human platelet GP Ib–IX complex in the absence of modulators. Genetic analysis of the vWF gene from patients with von Willebrand's disease has identified five point mutations (R543 → W, R545 → C, W550 → C, V553 → M, and R578 → Q) which appear to be responsible for the disorder (Cooney et al., 1991; Ware et al., 1991). Additional evidence that this highly basic region of the molecule is involved in the regulation of vWF adhesive activity is that the interaction between vWF and its modulator, botrocetin, is inhibited by synthetic peptides corresponding to the vWF sequences D514–E542, D539–V553, and K569–N583 (Sugimoto et al., 1991; Berndt et al., 1992).

It is therefore interesting to speculate that the nonconservative mutations which occur in Type IIb von Willebrand's disease, as well as the binding of the modulators botrocetin and ristocetin, might alter the orientation of the spatially proximal E527–V538 helical segment so that the charged face of the helix is exposed and recognized by the GP Ib–IX complex. Alternatively, the highly basic region downstream of vwf29 may be directly involved in electrostatic interactions

with the highly acidic segment of GP Ibα. Current studies are directed toward an examination of the the effects of the point mutations in Type IIb von Willebrand's disease on the solution conformation of the segment encompassed by vwf29.

ACKNOWLEDGMENT

We greatly appreciate the help of Dr. Peter Güntert with the DIANA and GLOMSA programs and Dr. David Norman with the X-PLOR program. We would also like to thank Mr. Keith Junius for assistance with the early structure calculations. Special thanks to Dr. Herman Schreuder for supplying a version of the SUPPOS program that is capable of handling protons.

REFERENCES

Ali-Briggs, E. T., Clemetson, K. J., & Jenkins, C. S. P. (1981) *Br. J. Haematol. 48*, 305–318.

Andrews, R. K., Gorman, J. J., Booth, W. J., Corino, G. L., Castaldi, P. A., & Berndt, M. C. (1989) *Biochemistry 28*, 8326–8336.

Basus, V. J. (1989) *Methods Enzymol. 177*, 132–149.

Bax, A., & Davis, D. G. (1985) *J. Magn. Reson. 65*, 355–360.

Berndt, M. C. (1989) *Today's Life Sci. 1*, 20–25.

Berndt, M. C., Du, X., & Booth, W. J. (1988) *Biochemistry 27*, 633–640.

Berndt, M. C., Ward, C. M., Booth, W. J., Castaldi, P. A., Mazurov, A. V., II, & Andrews, R. K. (1992) *Biochemistry* (preceding paper in this issue).

Brünger, A. T. (1990) *X-PLOR Version 2.1, User Manual*, Yale University, New Haven, CT.

Clore, G. M., & Gronenborn, A. M. (1989) *CRC Crit. Rev. Biochem. Mol. Biol. 24*, 479–564.

Cooney, K. A., Nichols, W. C., Bruck, M. E., Bahou, W. F., Shapiro, A. D., Bowie, E. J. W., Gralnick, H. R., & Ginsburg, D. (1991) *J. Clin. Invest. 87*, 1227–1233.

Ferrin, T., Huang, C. C., Jarvis, L. E., & Langridge, R. (1988) *J. Mol. Graphics 6*, 13–27.

Fujimara, Y., Titani, K., Holland, L. Z., Russell, S. R., Roberts, J. R., Elder, J. H., Ruggeri, Z. M., & Zimmerman, T. S. (1986) *J. Biol. Chem. 261*, 381–385.

Girma, J.-P., Meyer, D., Verweij, C. L., Pannekoek, H., & Sixma, J. J. (1987) *Blood 70*, 605–611.

Güntert, P., Braun, W., & Wüthrich, K. (1991) *J. Mol. Biol. 217*, 517–530.

Kabsch, W. (1976) *Acta Crystallogr. A43*, 922–923.

Marion, D., & Wüthrich, K. (1983) *Biochem. Biophys. Res. Commun. 113*, 967–974.

Mohri, H., Fujimara, Y., Shima, M., Yoshioka, A., Houghten, R. A., Ruggeri, Z. M., & Zimmerman, T. S. (1988) *J. Biol. Chem. 263*, 17901–17904.

Murata, M., Ware, J., & Ruggeri, Z. M. (1991) *J. Biol. Chem. 266*, 15474–15480.

Nilges, M., Clore, G. M., & Gronenborn, A. M. (1988) *FEBS Lett. 239*, 129–136.

Pastore, A., & Saudek, V. (1990) *J. Magn. Reson. 90*, 165–176.

Sakariassen, K. S., Bolhuis, P. A., & Sixma, J. J. (1979) *Nature 279*, 636–638.

Sugimoto, M., Mohri, H., McClintock, R. A., & Ruggeri, Z. M. (1991) *J. Biol. Chem. 266*, 18172–18278.

Titani, K., Kumar, S., Takio, K., Ericsson, L. H., Wade, R. D., Ashida, K., Walsh, K. A., Chopek, M. W., Sadler, J. E., & Fujikawa, K. (1986) *Biochemistry 25*, 3171–3184.

Ware, J., Dent, J. A., Azuma, H., Sugimoto, M., Kyrle, P. A., Yoshioka, A., & Ruggeri, Z. M. (1991) *Proc. Natl. Acad. Sci. U.S.A. 88*, 2946–2950.

Wüthrich, K. (1986) *NMR of proteins and nucleic acids*, John Wiley and Sons, New York.